University of Bath

Alternative formats
If you require this document in an alternative format, please contact:
openaccess@bath.ac.uk

Dexterous manipulation of microparticles using Bessel-function acoustic pressure fields

Charles R. P. Courtney, Bruce W. Drinkwater, Christine E. M. Demore, Sandy Cochran, Alon Grinenko et al.

Additional information on Appl. Phys. Lett.

CrossMark
click for updates

Dexterous manipulation of microparticles using Bessel-function acoustic pressure fields

Charles R. P. Courtney,[1] Bruce W. Drinkwater,[1,a)] Christine E. M. Demore,[2] Sandy Cochran,[2] Alon Grinenko,[1] and Paul D. Wilcox[1]

[1]*Department of Mechanical Engineering, University of Bristol, Bristol BS8 1TR, United Kingdom*
[2]*Institute for Medical Science and Technology, School of Medicine, University of Dundee, Dundee DD2 1FD, United Kingdom*

We show that Bessel-function acoustic pressure fields can be used to trap and controllably position microparticles. A circular, 16-element ultrasound array generates and manipulates an acoustic field within a chamber, trapping microparticles and agglomerates. Changes in the phase of the sinusoidal signals applied to the array elements result in the movement of the Bessel-function pressure field and hence the microparticles. This demonstrates ultrasonic manipulation analogous to holographic optical tweezers. The manipulation limits of the device are explained by the existence of unwanted resonances within the manipulation chamber. © 2013 American Institute of Physics. [http://dx.doi.org/10.1063/1.4798584]

The acoustic radiation force is a nonlinear wave phenomenon best known for levitation experiments developed to create micro-gravity environments[1] and containerless processing of centimetre scale objects.[2] Insects and small swimming organisms have also been levitated acoustically.[3,4] The application of standing acoustic waves for filtering or concentrating[5–7] and patterning[8,9] of microscale particles, including cells and bacteria in the size range $0.1-100\,\mu m$, has been described. Typically such devices operate in the $1-10$ MHz frequency range, corresponding to wavelengths of approximately 1500-150 μm in water. A 10:1 ratio of wavelength to particle size results in excellent particle localisation at the pressure nodes, and ratios of up to 150:1 have demonstrated localisation.[9] This makes acoustic tweezers complimentary to optical tweezers[10] as they are able to manipulate larger objects and cell agglomerates.[11]

Under Rayleigh-scattering conditions, the wavelength is larger than the particle size, and the acoustic radiation force due to a standing wave is governed by the spatial gradient of the acoustic pressure in the vicinity of the particle, i.e., $F = -\nabla U$, where U is a function of the wave energy, often called the potential energy landscape.[12] To date, standing waves have been used in all applications of acoustic radiation forces for particle manipulation as they result in orders of magnitude higher forces than progressive waves.[12] In plane standing waves, particles with densities and stiffnesses greater than the medium experience forces towards pressure nodes, with amplitudes dependent on their size; this is the basis for particle filtering and sorting devices.[13] The distribution of particles into various simple geometric patterns, including lines as well as square and hexagonal grids, has been demonstrated in the production of nanostructured materials[9,14] and engineered tissue.[15,16] The trapping patterns can be manipulated (i.e., nodal pattern stretched) by using changes in frequency[17,18] and amplitude.[19] Recently, it has

been shown that such patterns can be translated if the sources are acoustically matched to the fluid, by varying the relative phases of the counter propagating waves.[20,21]

Various attempts have been made to increase dexterity, by allowing individual microparticles or agglomerates to be trapped and manipulated independently. Wu and Du[22] suggested then realised[23] focused beams to create spatial gradients of acoustic pressure and hence trap particles. Particles were translated relative to a chamber by physically moving the focusing sources. Similarly, particles have been trapped in the high spatial gradients within the near field of a planar source.[24] More closely following optical tweezing, acoustic trapping has also been demonstrated in the high frequency, Mie scattering, regime in which the wavelength is smaller than the particle using focused[25–27] and zeroth-order Bessel beams.[28,29] Particles have also been trapped using a resonant field between an element of a linear array and a reflector and then translated by switching elements.[30]

Acoustic vortices are characterized by a phase dependence around an axis given by $\exp(im\theta)$, where θ is the azimuthal angle and the topological charge, m, is an integer that determines the number of 2π phase changes around the axis.[31] Helicoidal beams having the additional property of propagation along the central axis have attracted significant theoretical and experimental interest. In particular, it has been demonstrated that helicoidal beams can impart angular momentum to objects.[32–34]

Helicoidal beams with $m = 1$ have been generated at relatively low frequencies (100 kHz) using four piezoelectric plates driven sinusoidally with $\pi/2$ phase delay between adjacent plates.[35] Models indicate that a similar device, designed to operate at megahertz frequencies, could be used to trap microparticles.[36] However this approach, using propagating helicoidal beams, leads to radial pressure distributions with a nodal spacing of several wavelengths, resulting in relatively small gradients in the potential energy landscape hence necessitating large (MPa) acoustic pressures to produce moderate (pN) forces. The approach proposed in this letter generates a

a)Author to whom correspondence should be addressed. Electronic mail: B.Drinkwater@bristol.ac.uk.

stationary Bessel function field without axial propagation, with a nodal spacing of less than a wavelength, greatly increasing the potential gradients.

This letter demonstrates experimentally the generation of acoustic vortices, without axial propagation, and their application to microparticle manipulation. Our approach is to use a circular array of transducers, with appropriate drive signals, to generate and control the acoustic field and therefore create and move traps. The array-based device operates analogously to a holographic optical tweezer[37,38] and can thus, in principle, create complex acoustic fields to realise dexterous trapping and manipulation. Here trapping and manipulation is demonstrated with first order Bessel-function acoustic pressure fields.

In order to generate acoustic vortices in a fluid filled chamber, a 16-element circular array was fabricated from a piezoceramic ring (Fig. 1). An acoustic vortex with topological charge, m, will be generated if the sinusoidal drive signals are phased such that there is a ramp of $2m\pi$ phase delay around the array: i.e., if the relative phase, ϕ_n, of the signal applied to each of the N elements, $n = 1, 2, 3, \ldots, N$ is given by

$$\phi_n = \left(\frac{2m\pi(n-1)}{N}\right). \tag{1}$$

The resulting pressure field in the chamber approximates a Bessel function given by

$$p(r, \theta) = P_0 J_m(kr)e^{im\theta}, \tag{2}$$

where (r, θ) are polar coordinates with an origin at the center of the Bessel function, coincident with the center of the array for the phases given in Eq. (1), and P_0 defines the peak pressure amplitude and $J_m(x)$ is an mth order Bessel function of the first kind. Note that the forces on a particle in a pressure field given by Eq. (2) can readily be computed using Gor'kov's equations.[12] for $m = 1$, the central ($r = 0$) pressure node coincides with a velocity anti-node, ensuring that particles that are denser and stiffer than the fluid medium will experience a force acting to trap them at $r = 0$. Further pressure nodes form concentric circles around the center and are not coincident with velocity anti-nodes. The location of trapping in these regions depends on both the pressure and velocity contributions to the potential energy landscape, U. For the particles used in this work, the pressure contribution dominates and trapping of particles in concentric rings corresponding to the pressure nodes is expected. The origin of the generated Bessel function can be translated, to a target

position (r_T, θ_T), by applying further phase delays proportional to the distance r_n between the target position and each element n. An mth-order Bessel-function pressure field centered on (r_T, θ_T) is generated by using a sinusoidal drive signal with relative phase, ϕ_n', applied to each element

$$\phi_n' = \left(\frac{2m\pi(n-1)}{N} - kr_n\right). \tag{3}$$

However, where a finite number of elements are used aliasing effects restrict the distance which the target position can be moved from the array center while maintaining a pressure field of the form given by Eq. (2). A previous work by the current authors[39] showed analytically that the distance of the center of the pressure field from the center of the array was limited by aliasing to

$$r_T < \frac{1}{2}\frac{(N-m)}{\pi e}\lambda, \tag{4}$$

where λ is the acoustic wavelength in the fluid medium filling the chamber. For a 16-element array and a 1st order Bessel function ($m = 1$), $r_T < 0.88\,\lambda$.

Figure 1 shows the configuration of a 16-element array with a water-filled chamber used to demonstrate the manipulation of particles using first order Bessel functions. The device was fabricated from a piezoceramic ring (material: PZ27, Meggitt Ferroperm, Denmark) of internal radius, $R = 5.49$ mm, wall thickness $t = 0.87$ mm, and height $h = 1.60$ mm. The ring was backed with an absorbing backing layer (epoxy with 60% by weight alumina added) and diced into 16 elements of internal circumferential width 2.16 mm. The array was operated at $f_e = 2.35$ MHz, the first thickness extensional resonant frequency of the elements. This corresponds to a wavelength in water, $\lambda = 622\,\mu m$, and a central region of control of radius $r_T = 560\,\mu m$ (Eq. (4)). The pressure field generated by the array causes no force perpendicular to the plane of the ring, i.e., in the vertical direction when the ring is horizontal. Therefore, to prevent settling due to gravity, a resonant levitation stage was added, consisting of a piezoelectric plate below the chamber and a glass-coverslip reflector above. Operating at 2.45 MHz and 14 V$_{pp}$, this acted to trap the particles in horizontal planes one above the other, on which the circular array could act for manipulation.

Figure 2(a) shows trapping of 10-μm-diameter polystyrene spheres by the zeroth-order Bessel function pressure field generated by applying the same 12 V$_{pp}$ sinusoidal signals to all 16 elements (i.e., driven in-phase). As expected,

(a)

10.98 mm

(b)

Backing layer
(Alumina loaded epoxy)
Electrodes

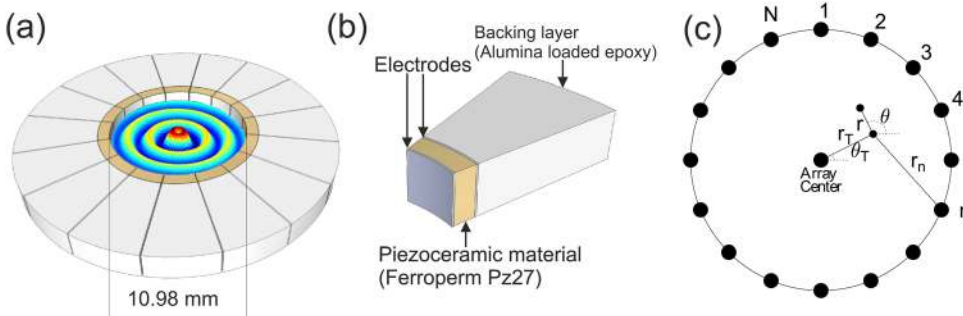Piezoceramic material
(Ferroperm Pz27)

(c)

Array
Center

FIG. 1. Diagrams of the experimental apparatus showing (a) the 16-element circular array device and the expected Bessel-function acoustic pressure field, (b) construction detail of one piezoelectric element of the array, and (c) a schematic of the device showing the coordinate system.
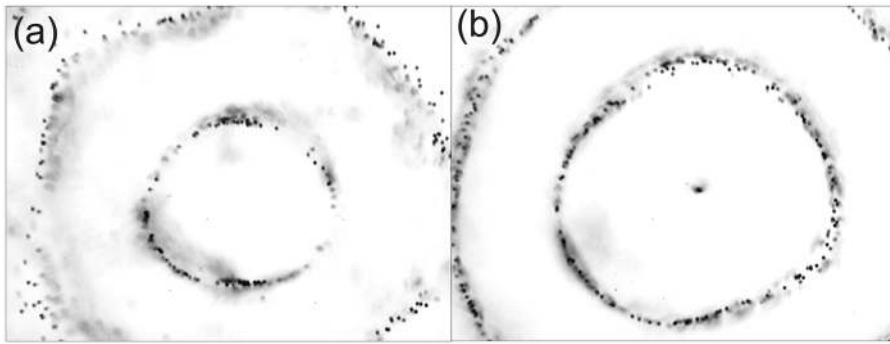
FIG. 2. Photographs of particles trapped using (a) a zeroth-order Bessel function of the first kind and (b) a first-order Bessel function of the first kind.
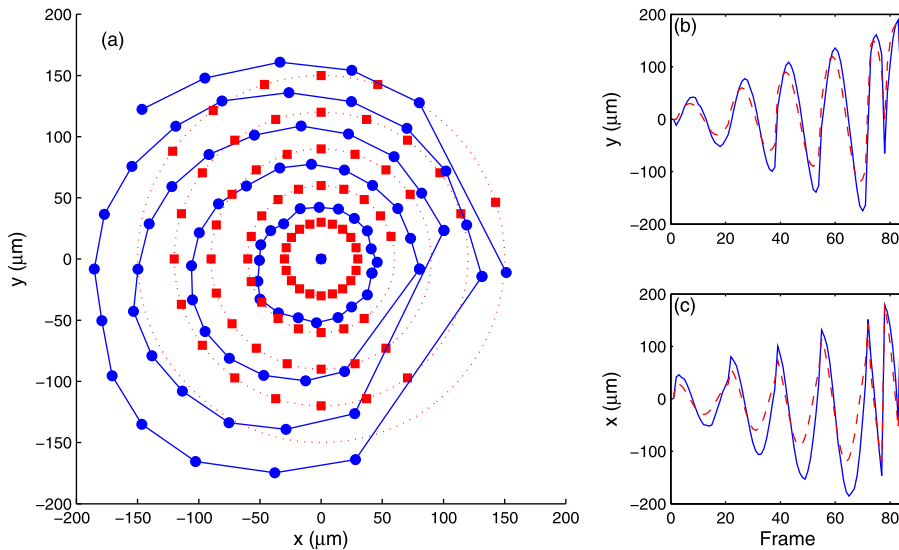

FIG. 3. Manipulation of $10\,\mu m$ polystyrene microspheres. The particles are manipulated in a series of five concentric circles. (a) shows the desired positions (dashed red line and squares) and the locations achieved experimentally when the device is controlled using Eq. (3) (blue circles). The outer set of experimental values is incomplete due to the trap failing. Insets (b) and (c) show the desired (dashed red) and experimental (blue solid) locations in the x- and y-directions, respectively.

the particles migrate towards the pressure nodes, which occur in a series of concentric rings. Figure 2(b) shows trapping of the particles at the center of a first-order Bessel function. Here, 12 V_{pp} sinusoidal signals were applied to the array elements with phases determined from Eq. (3) with $m = 1$ and $r_n = R$. A further circular trap at 0.61 λ (0.39 mm) corresponding to the second zero of the first-order Bessel function can also be seen.

The central trap in Fig. 2(b) can now be used to manipulate agglomerates. 10-μm-diameter polystyrene microspheres were added to the chamber and trapped vertically with the levitation transducer. First, the array was used to trap an agglomerate of 20 particles in the center of the chamber (12 V_{pp}, $m = 1$ and $r_n = R$). Second, using Eq. (3), the trap position was moved in a series of concentric circles of increasing radius (12 V_{pp}, $m = 1$). Figure 3 shows the achieved positions (r_R, θ_R) of the agglomerate center, with the target positions (r_T, θ_T) shown for comparison (see supplemental material[40]). The agglomerate can be manipulated up to $r_T = 160\,\mu$m, but the trap fails and the agglomerate is lost at greater distances. Figure 3 shows some discrepancy between the desired position (r_T, θ_T) and the actual position (r_R, θ_R) of the trap which is caused by the simplifying approximations used to derive Eq. (3), particularly the assumption of identical sources and negligible reflections within the chamber and the omission of any effects of the levitation field, which may not be entirely homogenous. An agglomerate of 7 particles, closely packed in a plane, was trapped and manipulated in a series of discrete steps (see supplementary material[40]). The peak velocity of the agglomerate was 65 μm/s, and

assuming that the motion is limited by the viscous drag and the agglomerate has an equivalent spherical diameter of approximately 20 μm, this indicates an acoustic radiation force on the agglomerate of the order of 10 pN.

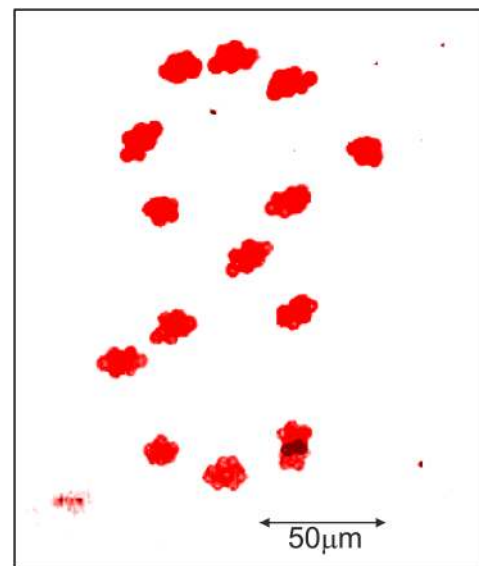More accurate manipulation requires either a more exact model, such as that considered by Grinenko *et al.*,[39] or some

FIG. 4. Manipulation of an agglomerate of $10\,\mu m$ polystyrene microspheres in a figure of eight. 14 separate photographs were summed to create this composite view. The contrast was adjusted and a false red colour added to aid viewing.
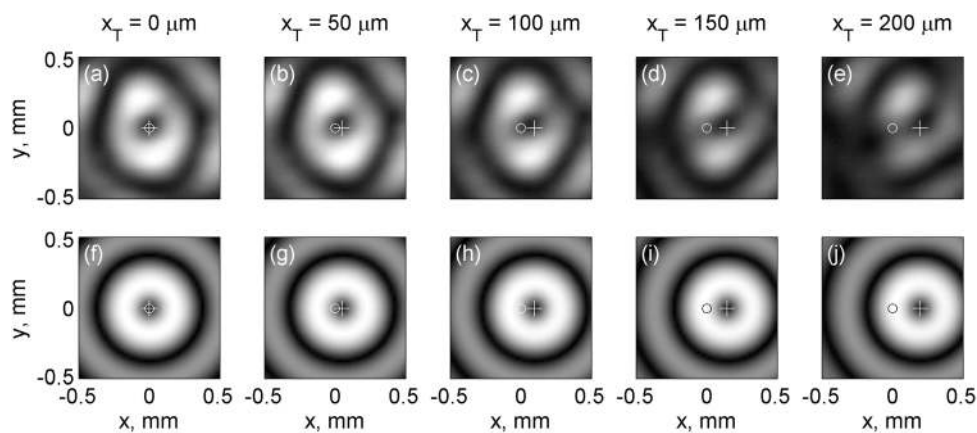
FIG. 5. Images of pressure field as target position (x_T, y_T) moves from center (0, 0) to (200 μm, 0 μm), along the line $y_T = 0$. (a)-(e) show schlieren images of the pressure field in the central 1 mm by 1 mm region of the chamber. The image is in a greyscale where black represents zero acoustic pressure and the maximum acoustic pressure amplitude is white; a circle has been superimposed at the chamber center, and cross marks the target position (x_T, y_T). The second row of images, (f)-(j), are pressure amplitudes calculated using a Huygens model, which accounts only for direct signals from the elements, ignoring boundary effects, including reflection.

form of feedback and adaption. The most straightforward feedback method, where trap positions are observed and then the drive signals adjusted manually, was used to move an agglomerate through a figure of eight, with a maximum dimension of 170 μm. The results are shown in the composite photomicrograph in Fig. 4. It is interesting to note that the agglomerate does not rotate and maintains an approximately fixed orientation with respect to the pressure field. We postulate that this is because a combination of imperfections in the generated Bessel field and the asymmetry of the agglomerate result in stable circumferential gradient forces that exceed the torque due to the acoustic vortex.

The translation of the origin of the Bessel function to (r_T, θ_T) is achieved if two conditions are met, one is that r_T obeys Eq. (4), and the second is that there are no reflections in the chamber. Reflections within the chamber build up into resonances with fixed nodal positions creating an unwanted acoustic pressure distribution that competes with the desired Bessel-shaped distribution. Figures 5(a)–5(e) shows five images of the central region of the fluid-filled chamber, as r_T is increased from 0 to 200 μm, taken with a schlieren optical system, which uses changes in refractive index to image the variation of acoustic pressure amplitude. For these measurements, the levitation transducer was removed and replaced with a transparent glass coverslip, to allow imaging through the chamber and the device was mounted vertically on an optical bench in the optical path of the schlieren system. For comparison, Figs. 5(f)–5(k) shows the normalised pressure amplitudes calculated using a Huygens' model. As this model includes only direct contributions for each element and excludes boundary effects, it represents the best possible approximation to a first order Bessel function possible for an idealised device using 16 elements. The schlieren images demonstrate that a trap, consisting of a pressure node surrounded by a pressure anti node, can be generated at the center of the trap. There is some non-uniformity in the trap and this grows as the trap is moved from the chamber center. This distortion is responsible for the loss of manipulation for $r_T > 160$ μm. Note that the wavelength at this frequency is 622 μm and so a simple planar standing wave across the chamber would result in unwanted traps at $r_T = 156$ μm ($\lambda/4$)

from the center. This agrees well with the experimental finding that trapping is difficult beyond $r_T = 160$ μm from the center.

In conclusion, it has been demonstrated experimentally that acoustic vortices can be used to trap agglomerates of 10 μm diameter microparticles in water. The pressure distributions were produced using a circular array of 16 piezoelectric elements. By application of appropriately phase delayed sinusoidal signals to the elements, the pressure field in the center of the array could be made to approximate a first-order Bessel function of the first kind centered at any point within 160 μm of the center. The position of agglomerates trapped in the central node of the pressure field was controlled by moving the center of the Bessel function. The region in which trapping is possible is limited in principle by the number of elements and in practice by resonance within the device. This suggests ways to improve the dexterity: increasing the number of elements to increase r_T, and adding acoustic matching and damping layers to reduce the unwanted geometric resonances.

[1]E. H. Trinh, Rev. Sci. Instrum. **56**, 2059 (1985).
[2]S. K. Chung and E. H. Trinh, J. Cryst. Growth **194**, 384 (1998).
[3]M. Saito, S. Izumida, and J. Hirota, Appl. Phys. Lett. **71**, 1909 (1997).
[4]W. J. Xie, C. D. Cao, Y. J. Lu, Z. Y. Hong, and B. Wei, Appl. Phys. Lett. **89**, 214102 (2006).
[5]F. Petersson, A. Nilsson, C. Holm, H. Jonsson, and T. Laurell, Lab Chip **5**, 20 (2005).
[6]M. Wiklund and H. M. Hertz, Lab Chip **6**, 1279 (2006).
[7]T. Laurell, F. Petersson, and A. Nilsson, Chem. Soc. Rev. **36**, 492 (2007).
[8]M. Saito, T. Daian, K. Hayashi, and S. Izumida, J. Appl. Phys. **83**, 3490 (1998).
[9]B. Raeymaekers, C. Pantea, and D. N. Sinha, J. Appl. Phys. **109**, 014317 (2011).
[10]A. Ashkin, J. M. Dziedzic, and T. Yamane, Nature **330**, 769 (1987).
[11]G. Thalhammer, R. Steiger, M. Meinschad, M. Hill, S. Bernet, and M. Ritsch-Marte, Biomed. Opt. Express **2**, 2859 (2011).
[12]L. P. Gor'kov, Sov. Phys. Dokl. **6**, 773 (1962).
[13]R. J. Townsend, M. Hill, N. R. Harris, and N. M. White, Ultrasonics **42**, 319 (2004).

[14]F. G. Mitri, F. H. Garzon, and D. N. Sinha, Rev. Sci. Instrum. **82**, 034903 (2011).

[15]A. L. Bernassau, F. Gesellchen, P. G. A. MacPherson, M. Riehle, and D. R. S. Cumming, Biomed. Microdevices **14**, 559 (2012).

[16]L. A. Kuznetsova, D. Bazou, G. O. Edwards, and W. T. Coakley, Biotechnol. Prog. **25**, 834 (2009).

[17]C. D. Wood, J. E. Cunningham, R. O'Rorke, C. Walti, E. H. Linfield, A. G. Davies, and S. D. Evans, Appl. Phys. Lett. **94**, 054101 (2009).

[18]X. Ding, S.-C. S. Lin, B. Kiraly, H. Yue, S. Li, I. K. Chiang, J. Shi, S. J. Benkovic, and T. J. Huang, Proc. Natl. Acad. Sci. U.S.A. **109**, 11105 (2012).

[19]A. Haake, A. Neild, G. Radziwill, and J. Dual, Biotechnol. Bioeng. **92**, 8 (2005).

[20]C. R. P. Courtney, C. K. Ong, B. W. Drinkwater, A. L. Bernassau, P. D. Wilcox, and D. R. S. Cumming, Proc. R. Soc. A **468**, 337 (2012).

[21]L. Meng, F. Cai, J. Chen, L. Niu, Y. Li, J. Wu, and H. Zheng, Appl. Phys. Lett. **100**, 173701 (2012).

[22]J. R. Wu and G. H. Du, J. Acoust. Soc. Am. **87**, 997 (1990).

[23]J. R. Wu, J. Acoust. Soc. Am. **89**, 2140 (1991).

[24]T. Lilliehorn, U. Simu, M. Nilsson, M. Almqvist, T. Stepinski, T. Laurell, J. Nilsson, and S. Johansson, Ultrasonics **43**, 293 (2005).

[25]J. Lee, C. Lee, H. H. Kim, A. Jakob, R. Lemor, S.-Y. Teh, A. Lee, and K. K. Shung, Biotechnol. Bioeng. **108**, 1643 (2011).

[26]J. Lee, S.-Y. Teh, A. Lee, H. H. Kim, C. Lee, and K. K. Shung, Appl. Phys. Lett. **95**, 073701 (2009).

[27]F. Zheng, Y. Li, H. S. Hsu, C. G. Liu, C. T. Chiu, C. Lee, H. H. Kim, and K. K. Shung, Appl. Phys. Lett. **101**, 214104 (2012).

[28]P. L. Marston, J. Acoust. Soc. Am. **120**, 3518 (2006).

[29]Y. Choe, J. W. Kim, K. K. Shung, and E. S. Kim, Appl. Phys. Lett. **99**, 233704 (2011).

[30]P. Glynne-Jones, C. E. M. Demore, C. W. Ye, Y. Q. Qiu, S. Cochran, and M. Hill, IEEE Trans. Ultrason. Ferroelectr. Freq. Control **59**, 1258 (2012).

[31]J. L. Thomas and R. Marchiano, Phys. Rev. Lett. **91**, 244302 (2003).

[32]C. E. M. Demore, Z. Yang, A. Volovick, S. Cochran, M. P. MacDonald, and G. C. Spalding, Phys. Rev. Lett. **108**, 194301 (2012).

[33]K. Volke-Sepulveda, A. O. Santillan, and R. R. Boullosa, Phys. Rev. Lett. **100**, 024302 (2008).

[34]K. D. Skeldon, C. Wilson, M. Edgar, and M. J. Padgett, New J. Phys. **10**, 013018 (2008).

[35]B. T. Hefner and P. L. Marston, J. Acoust. Soc. Am. **106**, 3313 (1999).

[36]S. T. Kang and C. K. Yeh, IEEE Trans. Ultrason. Ferroelectr. Freq. Control **57**, 1451 (2010).

[37]D. G. Grier, Nature **424**, 810 (2003).

[38]A. T. O'Neil, I. MacVicar, L. Allen, and M. J. Padgett, Phys. Rev. Lett. **88**, 053601 (2002).

[39]A. Grinenko, P. D. Wilcox, C. R. P. Courtney, and B. W. Drinkwater, Proc. R. Soc. London, Ser. A **468**, 3571 (2012).

[40]See supplementary material at http://dx.doi.org/10.1063/1.4798584 for the images used to generate the data and a video in real time.